

CYCLIC LOADING OF SANDS WITH PRECISE
MEASUREMENT OF DISSIPATED ENERGY

A report submitted in partial fulfilment
of the requirements
for the degree of
Master of Engineering
at the
University of Canterbury,
Christchurch,
New Zealand.

by

K. J. SIMCOCK

University of Canterbury,
February, 1981.

ABSTRACT

This report outlines an experimental investigation into the mechanism of liquefaction. The investigation is centred on the relationship between the pore pressure build up in a sand sample, and the energy input to that sample by a cyclic load.

Cyclic triaxial tests were used to establish the form, if any, of this relationship. A large portion of the duration of the experimental investigation was spent in developing a workable test procedure. The development continued with the construction of an electronic integrator specifically for the testing work. This device facilitated the recording of a plot of the pore pressure versus work input to the sample, continuously, throughout the duration of a test.

A simple theory enabling prediction of the pore water pressure response to a given energy input at a known confining pressure is proposed. Comparison of the theoretical results with the measured traces for five analysed tests indicates that there is some merit to this description of the mechanism of the liquefaction of sands.

The report concludes by emphasising this promise and suggesting that detailed future research along similar lines is needed.

ACKNOWLEDGEMENTS

The author wishes to thank all the following for their assistance with this project.

Dr. R. O. Davis for his encouragement during all stages of the project work. His constant involvement and obvious interest in the work helped considerably in making the project a most enjoyable and valuable experience.

The contribution of Dr. Berrill and Dr. Mullenger in following the project work with interest is also appreciated.

John Van Dyk spent many hours firstly constructing and altering the test machinery and then preparing and testing samples. His work both in and out of normal hours was responsible for ensuring that a reasonable experimental program was completed. Bill Gavars also assisted frequently in the construction of the test equipment. The work of all the technical staff is truly appreciated.

Peter and Meriel Boerlage are thanked for their assistance with late testing work, and for their help with the photographic work in this report.

Roy Edmundson, who designed and built the integrator circuitry is thanked for his interest in and availability during the problem stages of the testing program.

Financial assistance from the New Zealand Ministry of Works and Development is gratefully appreciated.

TABLE OF CONTENTS

	<u>PAGE</u>
ABSTRACT	i
ACKNOWLEDGEMENTS	ii
TABLE OF CONTENTS	iii
LIST OF FIGURES	v
CHAPTER 1	1
INTRODUCTION	1
Literature Review	1
Scope of Project	3
CHAPTER 2	4
THE EXPERIMENT	4
Equipment	5
Test Material	7
Experimental Method	8
(a) Sample Preparation	8
(b) Test Procedure	10
CHAPTER 3	13
RESULTS	13
Discussion of Typical Test Result	13
Test 6/12/80, Cell 1.	13
CHAPTER 4	17
ANALYSIS OF TEST RESULTS	17
Stage 1 of Analysis	17
Stage 2 of Analysis	17
(a) Theory Development	17
(b). Typical Fitting of Results	22
Analysis of a Typical Test	22
Test 6/12/80, Cell 1	22
A Summary of Test Results	23
Discussion	25

	<u>PAGE</u>
CHAPTER 5	
CONCLUSIONS	30
Conclusions	30
Recommendations for Further Work.	30
REFERENCES	31

LIST OF FIGURES

<u>FIGURE</u>		<u>PAGE</u>
1	A schematic diagram of the equipment layout.	5
2	The equipment arrangement in the Wykeham Farrance testing frame.	6
3	Grain size distribution curve for New Brighton sand.	7
4	The sample preparation procedure.	9
5	Close-up of dial gauge positioning for alignment control.	11
6	A typical loading pattern.	11
7	Pore pressure and load traces from a typical test as recorded on the chart recorder.	14
8	A typical load versus deformation plot.	14
9	The recorded pore pressure versus work trace for a typical test.	16
10	A summary presentation of the test data, Stress Ratio versus number of cycles to failure.	18
11	Illustration of a stress ratio presentation of data from another researcher.	18
12	A plot illustrating the effect of sample density on the stress ratio plot.	19
13	A typical experimental pore pressure trace fitted with an exponential curve.	24
14	An experimental pore pressure versus work trace fitted with an average curve.	24
15	Comparison of the predicted theoretical pore pressure versus work relationship with a result recorded during a typical test.	25
16	Theoretical and recorded pore pressure versus work relationships for four analysed tests.	26
17	Summary of all recorded experimental pore pressure-work responses fitted with average theoretical results.	27

INTRODUCTION

The liquefaction of sands has been a contributing factor in several engineering failures. The 1964 Niigata earthquake in Japan⁽¹⁾ featured several foundation failures attributable to liquefaction of underlying sand material. Dam failures, such as those of the Calaveras Dam in California in 1920⁽²⁾ and the Lower Van Norman Dam during the 1971 San Fernando earthquake⁽³⁾ have also been caused by liquefaction of support material. As a result, the mechanism of liquefaction has been studied in the hope of avoiding similar failures in the future.

Literature Review

The phenomenon of sand liquefaction has been studied by several groups of researchers throughout the past twenty years. Their investigations have isolated many of the properties which characterise the occurrence of liquefaction, without yet providing a complete understanding of the mechanism.

It is apparent that liquefaction occurs in loose saturated sand subjected to shearing deformations. Earthquake shaking, or a gradual buildup of strains within a slope are possible sources for the deformations. Under the loading, loose sand compacts. This compaction increases the pressure within the water saturating the pores of the sand skeleton. Increasing the neutral (porewater) stress decreases the effective stress within the sand. When the effective stress is reduced to a level at which the sand structure is no longer able to resist the shearing forces, the sand is said to have liquefied.

Several schemes have been used to model this behaviour. These schemes have followed two distinct lines of analysis. The first approach involves observation of in-situ sand deposits. In particular the behaviour of sands during earthquakes is observed. After the Niigata earthquake of 1964⁽¹⁾, a number of Japanese engineers^(4,5,6) studied the areas in which liquefaction had or had not occurred. From their work, certain empirical criteria based primarily on the Standard Penetration Resistance of the sand deposits, were developed. These criteria differentiated between liquefiable and non-liquefiable conditions in Niigata. Using the Japanese idea as groundwork, other researchers, notably Seed and Peacock⁽⁷⁾, looked at relationships between field stress ratios of the form τ/σ (τ =horizontal shear stress, σ = initial effective overburden pressure) and sand relative density, again based on

standard penetration tests. Analysis of field cases is still continuing along similar lines, increasing the data base from which the empirical liquefaction formulae are derived.

The second analysis approach is one step more refined, linking field stresses with the threshold liquefaction stresses determined in laboratory experiments. Seed and Idriss⁽¹⁾ pioneered this analytical approach with their work on the Niigata earthquake. Adopting this approach requires an understanding of the development of stresses in potentially liquefiable layers in the ground, as well as the ability to produce a suitable test procedure for the determination of liquefaction stresses in the laboratory. Considerable work is being, and has been done in this field, with the aim of getting a deeper insight into the problems of liquefaction.

Analytical methods have developed with this work. The earliest research centred on development of stress-strain relationships for sand.⁽⁸⁾ These relationships evolved from studies of factors such as grain characteristics, previous strain history and relative density, which were known to affect the liquefaction potential of a sand sample. Effective stress analysis methods were the next development.⁽⁹⁾ In this form of analysis, the resistance to deformation at any point in the sand deposit is a function of the effective stress. This in turn depends on the rate of generation and dissipation of porewater pressure. The first attempts at this form of analysis by Finn et al.⁽⁹⁾ required the simplifying assumption that the individual sand layers were saturated and undrained, with no allowance for redistribution of porewater pressures between layers.

Seed, Martin and Lysmer⁽¹⁰⁾ were able to extend the theory in their paper of 1976, without requiring the drainage assumption. Their work used a finite difference scheme to simultaneously solve for the spatial and temporal variation of excess pore pressure. The scheme used a modified form of Terzaghi's one dimensional consolidation theory, with the addition of a term to account for the rise in pore pressure due to the shaking effects of an earthquake. After idealising the earthquake motion in an equivalent number of uniform cycles, the finite difference scheme could be used to predict the excess pore water pressures likely to develop in the soil deposit. The approach was a simple one, effective in predicting the pore water pressure values, without isolating the mechanism of the pore water pressure behaviour.

It was Oh-Oka⁽¹¹⁾ and Nemat-Nasser and Shokooh⁽¹²⁾ who made the next step forward in the study of liquefaction. Their observation that the densification of a sand prior to liquefaction involved a rearrangement of the grains and hence the expenditure of a certain amount of energy, led them to postulate a theory linking the energy loss in cyclic shearing to the consequent change in void ratio and rise in pore pressure in the saturated undrained case. Investigations into the energy-pore pressure relationships of Oh-Oka and Nemat-Nasser are still continuing.

Scope of Project

Many experimental techniques have been used in the past to determine liquefaction parameters. Cyclic simple shear tests, torsion ring and cyclic triaxial tests are just some of the experimental procedures which have been used.

In the work described below, a cyclic triaxial test procedure was developed, which enabled the preparation and testing of sand samples in an effort to investigate the relationship between pore pressure generation during cyclic loading and the amount of energy dissipated by the sand. A description of the experimental work performed and the apparatus used makes up Chapter 2 of this report. Chapter 3 presents a test history and discusses the various plots and traces which form the data from a typical test sample. Analysis of the results follows in Chapter 4. Included in the analysis, is a development of the theory from which the project was derived. The theoretically predicted results are then compared with the average experimental effects, to establish the validity of the proposed theory. The conclusions drawn from the project work are presented in Chapter 5, along with suggestions for areas of research in the future.

THE EXPERIMENT

Laboratory testing has been an integral part of the development of many of the modern theories relating to the mechanism of liquefaction. Although many testing methods have been tried, the most widely and successfully used procedure has been the stress controlled cyclic triaxial test.

The cyclic triaxial test involves assembling a specimen in a conventional triaxial cell and submitting it to cycles of uniform extension and compression strokes. The cyclic loading is generally achieved by either one of two methods. ⁽¹⁵⁾

- (a) Pneumatic Piston - A double acting piston is coupled to the specimen and the pressure or load is varied by selection through a directional solenoid valve.
- (b) Electrohydraulic Closed Loop - The double acting hydraulic piston is coupled to the specimen, with the piston action being controlled by an electronic servo valve.

Several papers ^(16,17,18,19) have been written with the intention of establishing performance specifications to enable researchers throughout the world to test varied material on different equipment, with some degree of consistency. Although a testing standard would be desirable, the diversity of equipment currently in use and the rapid advances in this area of research make such a proposal inappropriate. Rather, most writers ^(16,17) have limited themselves to discussing such aspects as alignment of the load cell-specimen system, recommended measuring devices, test cyclic frequency and other specialised test components and procedures.

A particular problem in cyclic triaxial testing is the preparation of consistent samples. Many preparation methods have been tried, ^(17,18) each giving a degree of consistency between similarly prepared samples, but with some variation in results between different preparation methods. Careful control is required in any testing program to ensure that consistency of sample properties is achieved, and reliable results obtained.

The remainder of this chapter describes the development of the test procedure and sample preparation methods used during the testing program.

Equipment

A schematic representation of the apparatus set up can be seen in Figure 1. Most of the equipment shown is typical of that used in liquefaction experiments. The exception here is the presence of the electronic digital integrator. Its main function was the automatic calculation of the work input to the sample being tested. To do this the integrator continuously added the input load and displacement signals, outputting the integrated result, the work signal. Also incorporated within the integrator circuitry were the power supplies for the load cell and displacement measuring LVDT.

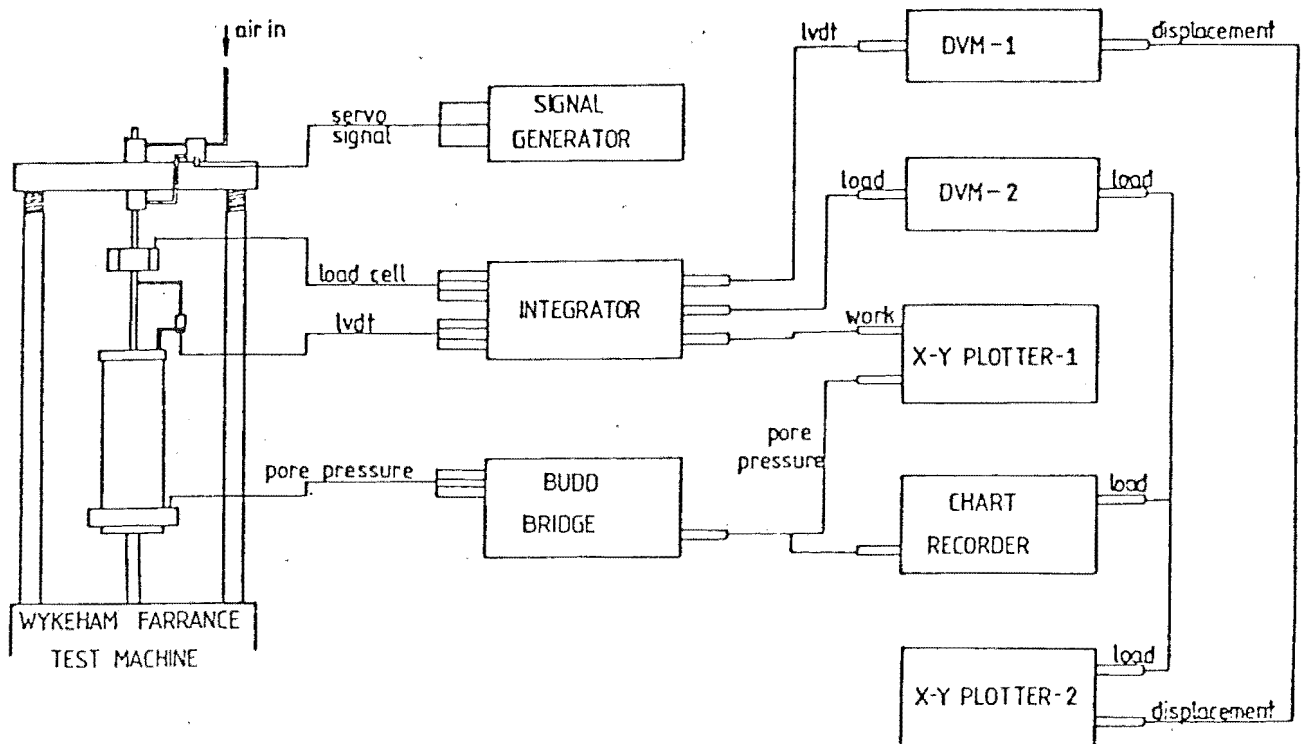


FIG. 1 A schematic diagram of the equipment layout.

The LVDT was mounted on the testing frame as shown in Figure 2. Its mounting position enabled it to record the relative displacements of the sand sample and the surrounding triaxial cell. This measurement was precisely the amount of axial deformation in the sample.

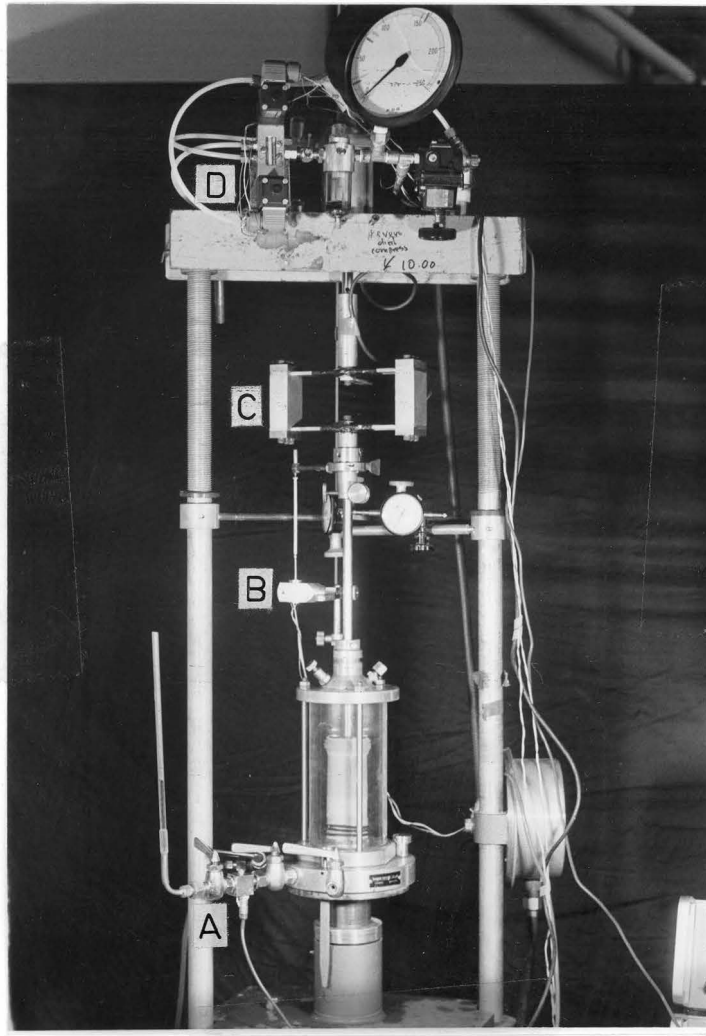


FIG. 2 The equipment arrangement in the Wykeham Farrance testing frame.

- A: Pore pressure transducer and measurement of volume change apparatus.
- B: LVDT device for measurement of sample deformation.
- C: Load cell.
- D: Pneumatic piston and air system for cyclic loading of sample.

A pressure transducer attached to the triaxial cell itself measured the pore pressure buildup within the sample during a test. A Budd bridge was used to convert the transducer output to a usable electronic signal.

The various output signals were monitored on the digital voltmeters, Hewlett Packard X-Y plotters and a 2 channel Toa chart recorder. The chart recorder's function was to provide a continuous record of the load applied to the sample, and the resulting pore pressure changes within that sample. Two X-Y plotters were used. The first of these recorded a load versus deflection plot, whilst the second plotted pore pressure versus work input to the sample. The digital voltmeters were used only at the beginning of a test. Their recordings were used to obtain appropriate zero readings for the load cell and the LVDT. This process is described more fully later in this chapter.

Test Material

The sand tested throughout the laboratory program was a uniform beach sand known as New Brighton sand. Its grain size distribution curve can be seen in figure 3. Tests performed on the washed sand produced a maximum void ratio of 0.965, and a minimum value of 0.606.

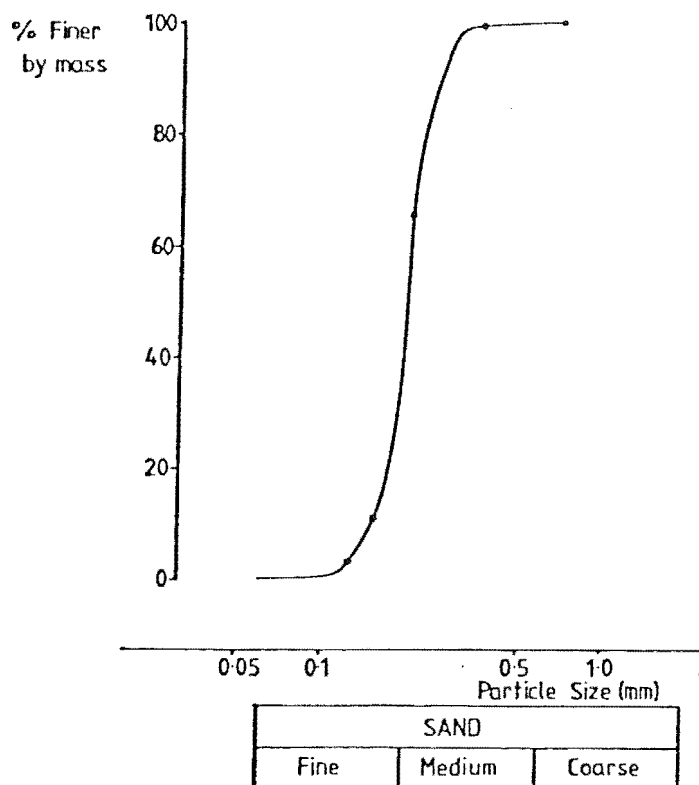


FIG. 3 The Grain Size Distribution Curve for New Brighton sand. This sand was used for all the samples tested.

Experimental Method

Sample Preparation

Considerable experimentation was required before a preparation procedure which resulted in samples of consistent density was found. The method finally adopted was as follows.

A metal former was assembled on the triaxial cell apparatus, surrounding a standard 1.5 inch rubber membrane. A porous stone was placed inside the former at the base end of the sample. Sand with a dry weight of 145 g was then poured into the water filled mould. The use of the water filled mould enabled the sand grains to settle gently, without developing a density gradient along the length of the sample. After the pouring was finished, the sample was tamped using a 15 mm diameter rod. Experience determined the number of tamps necessary to produce a desired sample density. The sample was next placed in a vacuum dessicator and de-aired under vacuum for a minimum of 5 hours. It was found that such a period was sufficient to ensure that the sample was fully saturated. The absence of air bubbles being drawn from the sample was considered to be evidence of saturation.

Following saturation, the top end of the sample was sealed around the loading piston, using three rubber rings. At this stage an initial suction was applied to the sample, to stiffen it slightly and provide some protection against disturbance during later handling. The metal former was then removed, and the sample diameter measured. Diameters were measured at three separate cross-sections using a travelling telescope device. Sightings were made to the outside edge of the rubber membrane confining the sample. Subtraction of twice an average membrane thickness resulted in the sample diameter, a result which was expected to be determined to better than 0.1 mm. At this stage, the sample height was also measured, using vernier calipers in the manner shown in figure 4.

The complete triaxial cell was then assembled. Locking collars on the top of the cell ensured that the sample would not be disturbed by subsequent handling. A second measurement of the sample height was made after the cell was put together, to check that the assembly process had not shortened the sample. If a difference greater than 0.2 mm was found between the two height readings, the sample was assumed to have been disturbed, and any results from subsequent testing were not considered valid. After this check the specimen was considered ready for testing.

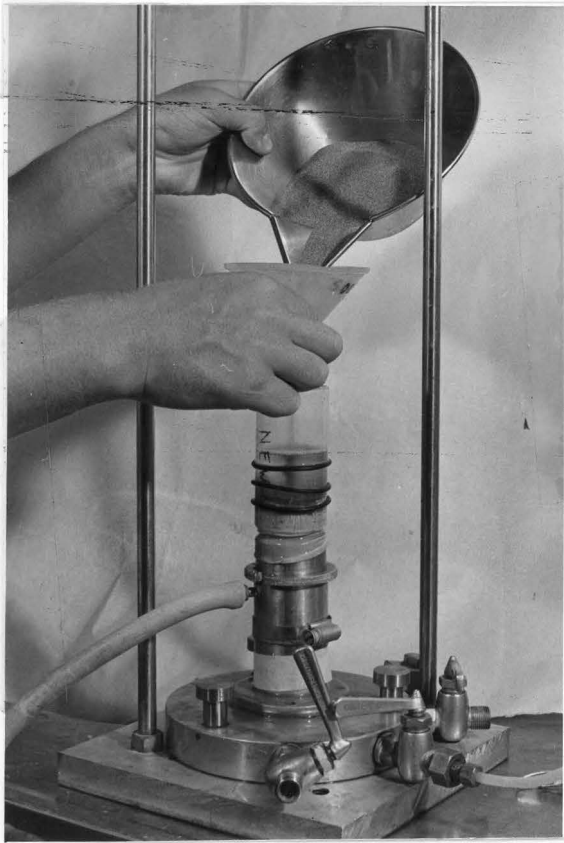


Fig. 4(a) - Sand (145 g dry weight) is poured into the water filled rubber membrane.



Fig. 4(b) - The saturated sample is clamped rigidly and its measurements recorded.

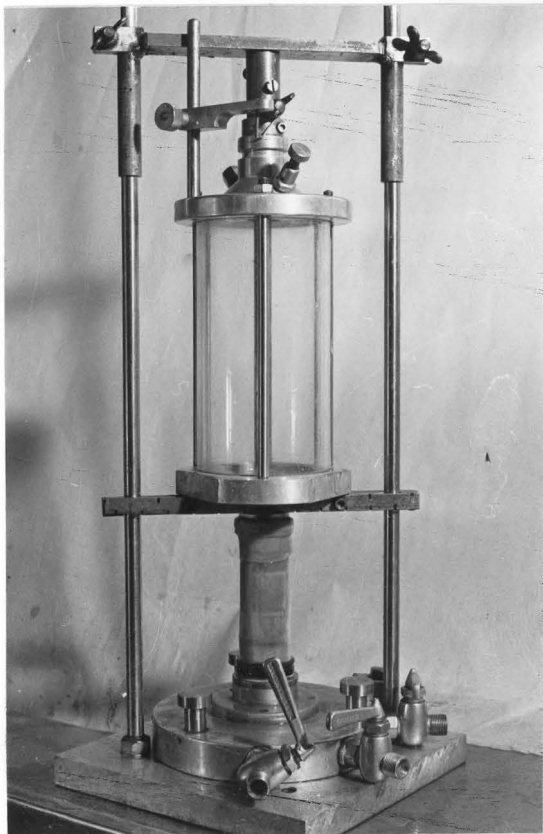


Fig. 4(c) - The triaxial cell is assembled, with the sample rigidly clamped.

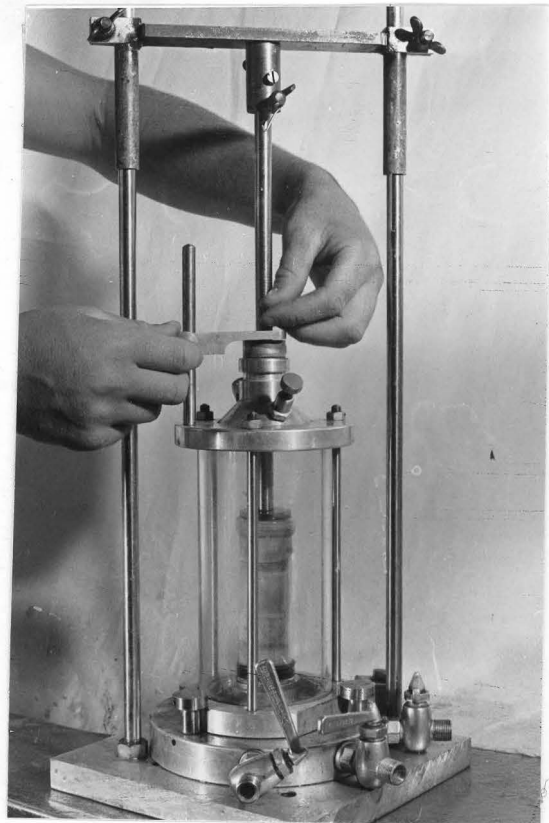


Fig. 4(d) - Assembly of the cell is completed by the fixing of the locking collars.

Fig. 4 - The sample preparation procedure.

Test Procedure

The prepared triaxial cell was first clamped into the testing frame. An initial 50 kPa confining pressure was applied, and the corresponding change in sample volume recorded. The volume change was recorded using the standard burette approach.⁽²¹⁾ This method required drainage of the sample, removing the initial suction applied during the preparation procedure. The cell pressure was increased in further 50 kPa stages until the desired test confining pressure was reached. At each stage the sample volume change was recorded.

After checking that all the monitoring equipment was correctly connected, the load cell was coupled to the triaxial cell piston. This step proved to be a critical feature of the cell set up.

To seal the top of the triaxial cell against loss of internal confining pressure, the cell piston passed through a brass gland. To minimise the frictional losses of piston force within this gland, the alignment of the piston-load cell connection was made with great care. It was found that a 0.1 mm variation of the piston from the vertical created significant frictional force. To avoid this problem, piston alignment was checked using two dial gauges, placed at right angles to each other, (Figure 5). Repeated tests, cyclically moving the piston shaft with no sample in the cell, refined the alignment technique to a degree where frictional effects could not be measured on any of the load records obtained in a test.

Having correctly aligned and set up the cell, the next requirement was to organise the recording apparatus. As previously shown, (Figures 1 and 2) the major information gathering pieces of equipment were the load cell, LVDT and the pore pressure transducer.

Before finally connecting the cell piston to the load cell, it was necessary to zero the output signal from the cell. This was done using a trim potentiometer in the integrator circuitry. Some creep was evident in the load cell signal initially, but a half hour warm up period ensured that this was reduced to a value of less than 0.01 N/min.

The displacement LVDT was next set in a zero position. After the first series of tests it was noticed that the samples tended to undergo greater extension than compression. Therefore, to best utilise the limited travel

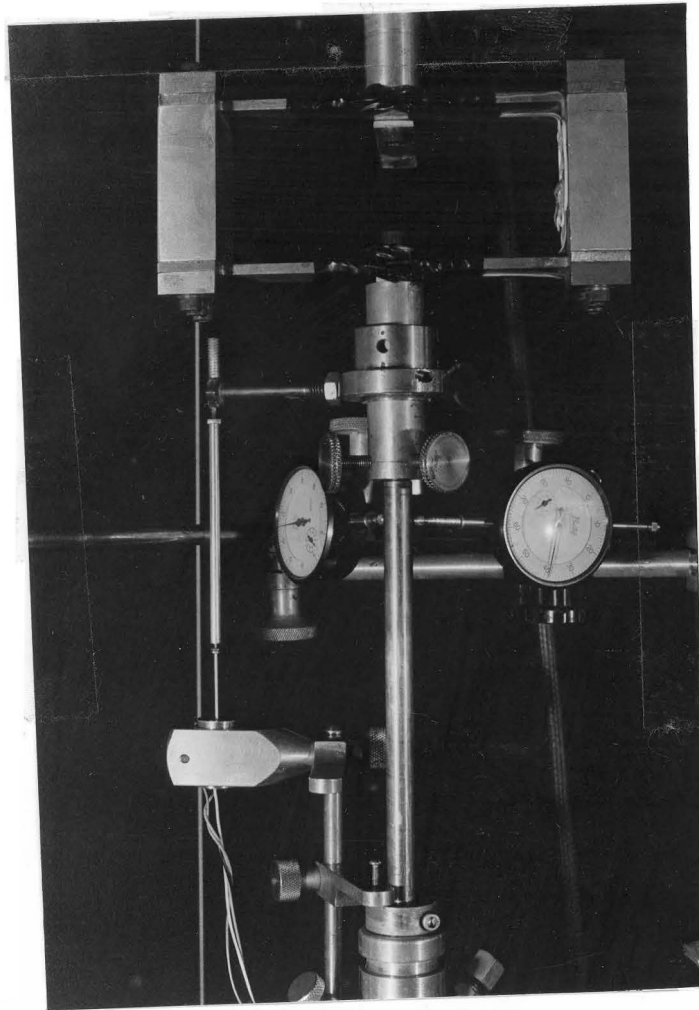


FIG. 5 A close-up view of the two dial gauges used to align the cell piston exactly with the load cell axis. The LVDT and load cell can also be seen.

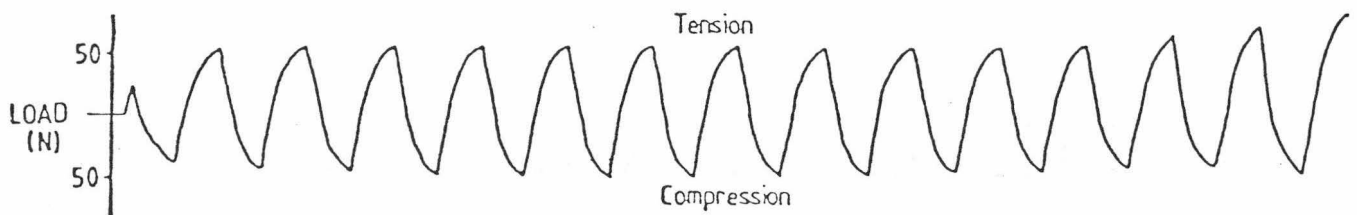


FIG. 6 A typical load trace as recorded on the chart recorder. The pattern is approximately sinusoidal.

of the LVDT the zero output signal of this device was biased 1 to 4 toward the compression side. This enabled sample axial extensions of up to 20 mm and compressions up to 5 mm to be recorded.

Setting up the pore pressure transducer required little work. The Budd bridge was balanced before the first series of tests, and checked before each test. It did not need any alteration during the test program.

Generally, tests were started with the sample experiencing a compressive stroke. The magnitude of the stroke was controlled by the air pressure supplied to the pneumatic ram. Experience was used to decide on a suitable air pressure for each test. It was also possible to alter the wave shape of the loading pattern by choking the exhaust valves of the air piston. After several trial runs a load pattern resembling a sinusoidal wave was adopted, (Figure 6).

Tests were continued until the displacement LVDT exceeded its range of travel. At this point all measuring systems were switched off, and the tri-axial cell removed from the testing frame.

Because some of the sand was lost during the preparation procedure, the mass of sand sample actually tested was carefully recovered from within the rubber membrane. This sand was oven dried with the dry weight being used in all subsequent analysis of test results. In general, less than one percent (dry weight) of sand was lost during sample preparation, testing and recovery.

RESULTS

The test program involved 32 tests run at 3 different confining pressures. Most of the tests were run at 100 kPa confining pressure, 19 records having been obtained from these tests. A further 7 tests were run at 150 kPa cell pressure, with 6 tests run at 50 kPa confining pressure. Although 32 tests were run in total, some test results are suspect because of equipment and set up problems at the time of testing. In particular, the 100 kPa cell pressure was used during the initial familiarisation period. As a consequence 5 of the tests run in this series experienced problems such as equipment not connected, earthing short circuits and poor pen performance. One of the tests run at 150 kPa also showed evidence of poor electrical connections in the pore pressure line, resulting in a suspect pore pressure trace. The 50 kPa tests were the final series run. No obvious problems were experienced during the testing of these samples.

It was evident from the traces produced during the cyclic triaxial tests that there were similarities in behaviour for samples with similar measured properties. A discussion of the features observed in one typical test follows.

Test 6/12/80, Cell 1

Figure 7 shows a typical chart recorder trace with a loading pattern starting with a small extension pulse. The majority of tests were started with a compressive stroke, but some samples experienced an initial extension cycle. It was characteristic of the test loading to find unequal extension and compression amplitudes. Unfortunately it proved impossible to exactly balance the cyclic loads with the loading system used. Counterweights to correct the unequal loads worked to a limited degree, but did not compensate sufficiently to fully balance the setup. It was also characteristic of the load trace to find a progressive increase in the force amplitude during the first four or five cycles. This was thought to be due to the slow buildup to the required pressure in the pneumatic system.

The lower half of Figure 7 is the trace from the second channel of the chart recorder. This shows the pore pressure response to the applied loading pattern. As can be seen, each load stroke causes a corresponding change in the pore pressure within the sample. Compressive strokes increase the pore pressure whilst extension strokes have the opposite effect. In general the

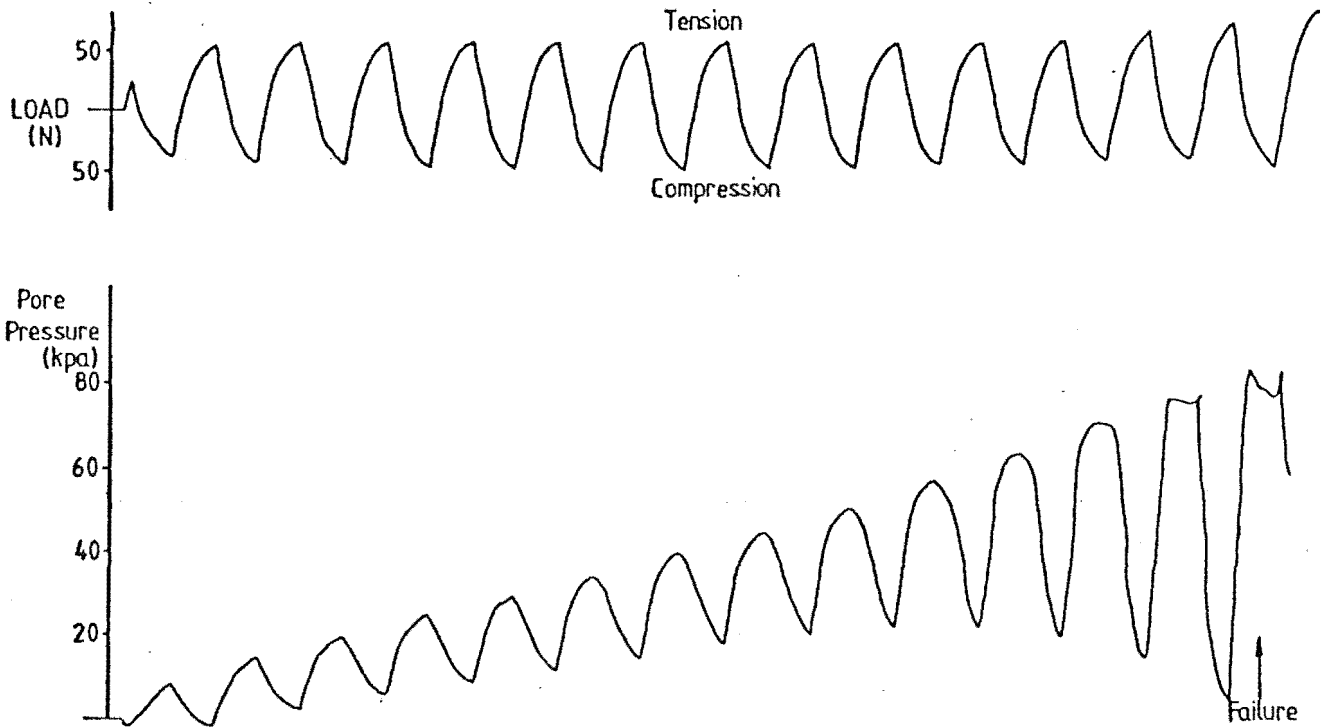


FIG. 7 Typical test results for the traces obtained from the chart recorder. The top trace is the loading pattern for the test, whilst the bottom trace represents the pore pressure response of the sample.

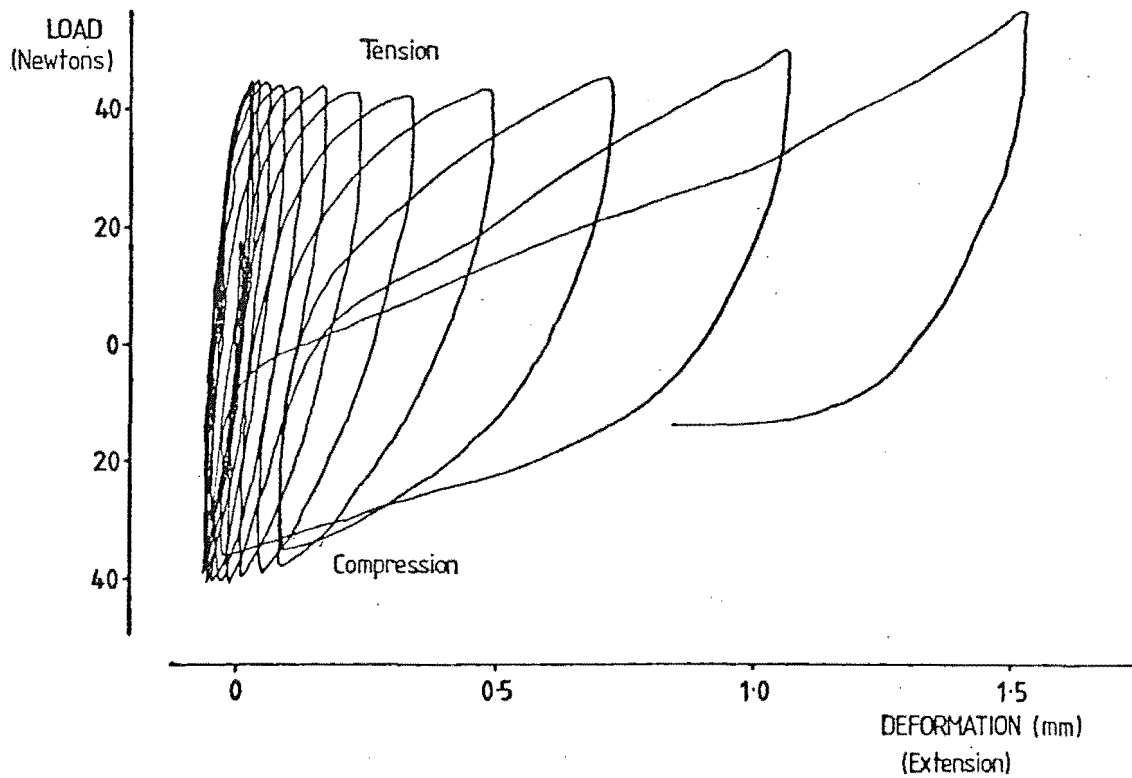


FIG. 8 The load versus deflection trace from the typical test.

increases due to compression were of greater magnitude than the decreases due to extension, resulting in a nett increase in pore pressure over the duration of one complete load cycle. The pore pressure builds up until some limiting value is reached, and the sample liquefies.

The definition of failure (or liquefaction) of a sample was arbitrarily based on the pore pressure response. This feature was considered to be relevant because it pictorially traced one of the known properties of the mechanism of liquefaction. Failure was considered to have occurred in the first cycle which showed a sudden decrease followed by a more sudden increase in the pore pressure response to a compressive stroke, (see Figure 7).

Figure 8 illustrates the force versus deformation response for this typical test. It can be seen that the initial load cycles cause little deformation of the sample. As the cycles continue and the load reaches its constant value, the sample begins to deform, extending in length. The rate of extension increases as the loading continues, indicating a softening of the sample structure before its liquefaction. The slope of the line A-B for each of the hysteresis loops also portrays the sample softening effect. Initially the loops are upright with an almost infinite slope. As the test proceeds the loops increase in size and the slope decreases. If this slope is considered as a measure of the stiffness of the sample, the progressive slope decrease is indicative of a softening of the sample.

The area under the force deflection plot is a measure of the work input to the sample. As discussed earlier, a continuous trace of this work input was provided by the electronic integrator specially constructed for the test program. The pore pressure response was plotted against the work output provided by the integrator, as shown in Figure 9. The shape of this plot appeared to be characteristic for all tests run at similar confining pressures. The pore pressure buildup under the applied loading is apparent in this trace. Also apparent is the buildup of work input to the sample over the test duration. Some work recovery is evident in the sample response, but the overall effect is an increasing energy dissipation per cycle, again reflecting the softening of the sample.

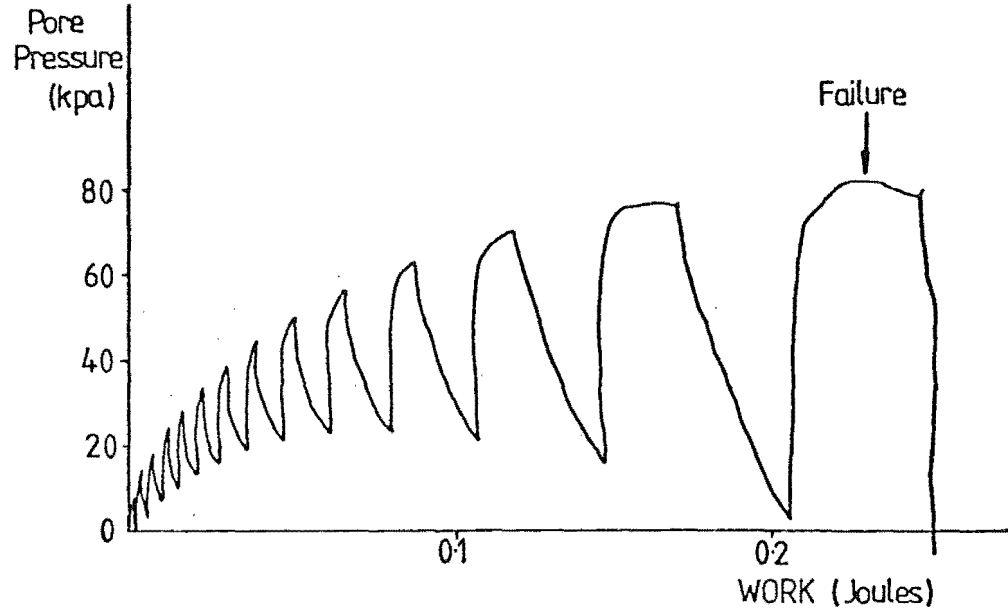


FIG. 9 A representation of a typical pore pressure versus work trace as recorded during a test.

ANALYSIS OF TEST RESULTS

Test results were analysed in two stages. The first stage was to express the experimental data in a form typical of that used by other researchers.^(7,16,18,19,20) Stage two involved reducing the information from the tests in an attempt to investigate the relationship between pore pressure buildup and dissipated energy.

Stage 1 of Analysis

Typically, liquefaction results have been written up using a dimensionless stress ratio plotted against the logarithm of the number of cycles to failure. Figure 10 is such a plot for the data obtained during the test program. The stress ratio used was that defined by Silver et al⁽¹⁶⁾,

$$SR = \frac{F_c + F_e}{4 \sigma_c A_c} \quad (1)$$

where F_c and F_e represent the applied compression and extension loads, σ_c denotes the cell confining pressure and A_c is the consolidated area of the sample.

In their paper, Silver et al suggested that samples of similar relative densities should be on a line of the form shown in Figure 11. It was further suggested by Mulilis et al⁽¹⁹⁾ that denser specimens should show a similar trend, but at greater values of the stress ratio for a similar number of cycles to failure, (Figure 12). Comparison of these results with Figure 10 reveals that the trend described by the writers is apparent. It is also clear however, that there is considerable scatter in the results and an average effect only exists. The scatter in Figure 10 is not excessive relative to that in Figure 11.

Stage 2 of Analysis

Theory Development.

The theory being tested related the total work input to a sample at a given number of cycles to the pore pressure within the sample at that cycle. The work of Davis and Mullenger⁽¹³⁾ suggests that the increase in pore pressure, Δu , during a loading stroke, (either extension or compression) with peak

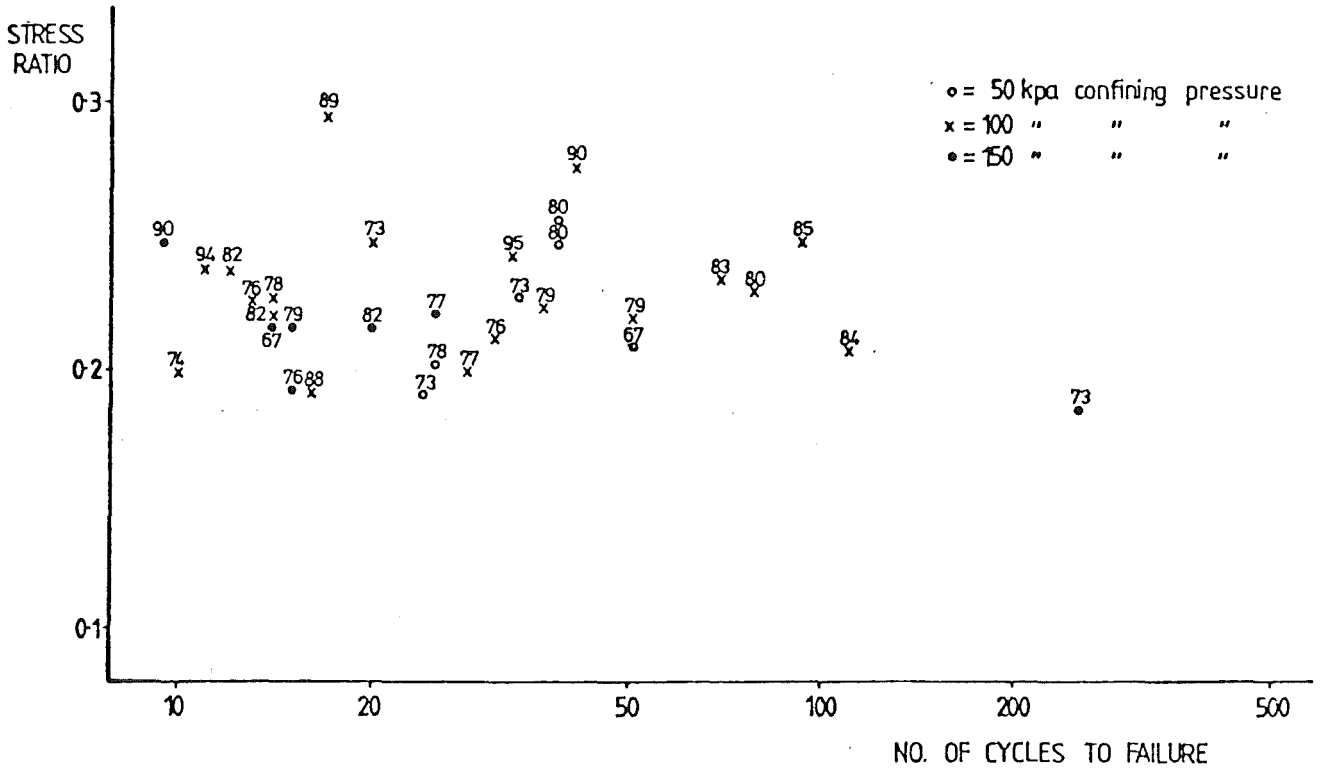


FIG. 10 A plot of stress ratio versus number of cycles to failure for all the experimental data.

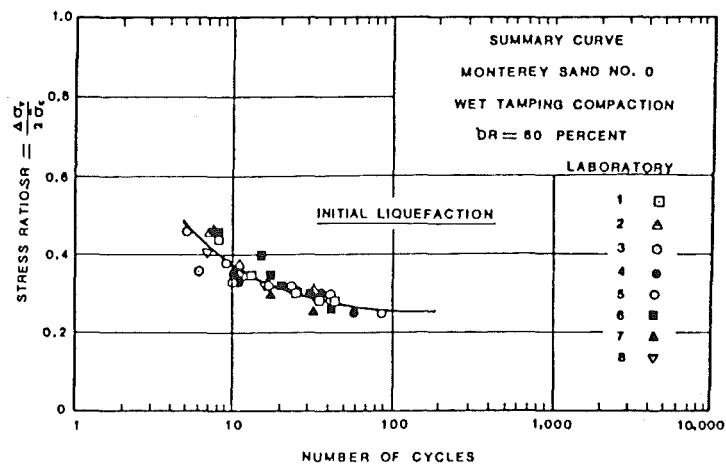


FIG. 11 The typical stress ratio plot for experimental data. (after Silver et al⁽¹⁶⁾).

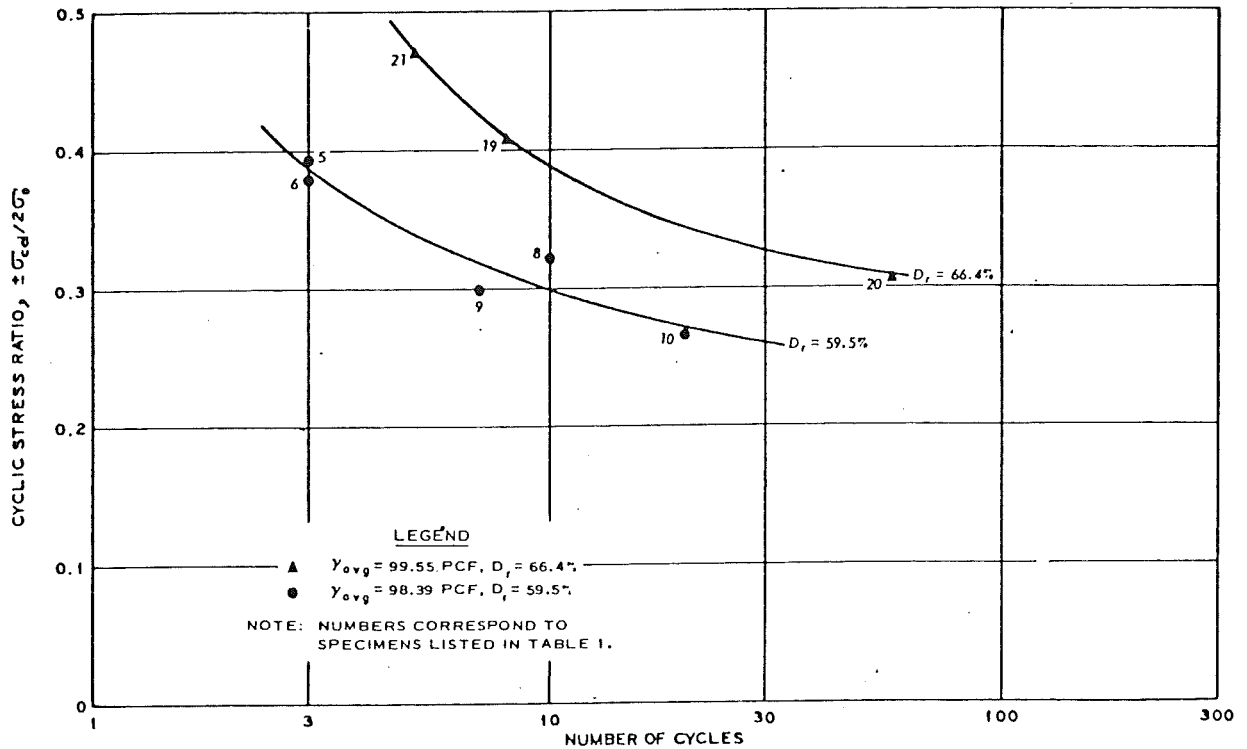


FIG. 12 An illustration of the effect of sample density on the stress ratio for a series of experimental results. (after Mulilis et al⁽¹⁹⁾).

deviatoric stress q , is given by,

$$\Delta u = (p_1 - p_c) \left[1 - \exp\left(-\frac{q_1^2}{2M^2}\right) \right] \quad (2)$$

Here p_1 represents the mean effective stress at the beginning of the cycle, p_c denotes the critical state mean stress (for example see Schofield and Wroth⁽²²⁾) and $M (= M_0 p_c)$ represents the failure stress for the sample. The corresponding work dissipated during the cycle, ΔW , is given by,

$$\Delta W = \frac{M^2}{4\mu} \left[\ln \left(\frac{M^2}{M^2 - q_1^2} \right) - \frac{q_1^2}{M^2} \right] \quad (3)$$

where $\mu = \mu(p)$ is the shear modulus of the sand. By treating the finite differences of u and W in (2) and (3) as approximate differential equations, the two equations may be combined to yield the following differential equation,

$$\frac{du}{dW} \approx \frac{\Delta u}{\Delta W} = \frac{(\sigma_c - u - p_c) [1 - \exp(q_1^2/2M^2)]}{\frac{M^2}{4\mu} \left[\ln \left(\frac{1}{1 - (q_1/M)^2} \right) - \left(\frac{q_1}{M} \right)^2 \right]} \quad (4)$$

Here the mean effective stress p_1 has been replaced by $\sigma_c - u$. It is important to note that the differential equation is an approximate expression only for the average or middle response of u versus W . In (4), q_1 and σ_c are constants which can be measured directly. M and p_c are also constants which need to be determined if the above expression is to be integrated. To obtain values for M and p_c , equation (2) and the pore pressure time history were used. Equation (2) can be rewritten as,

$$\Delta u = B(A+u) \quad (5)$$

where $B = \exp(q_1^2/2M^2) - 1$ (6)

and $A = p_c - \sigma_c$ (7)

If it is assumed that the chart recorder moves with constant velocity v , and we let L_c be the length of chart used in tracing a single cycle, then the time for one cycle is,

$$\Delta t = L_c/v \quad (8)$$

Combining (5) and (8) gives,

$$\frac{du}{dt} \approx \frac{\Delta u}{\Delta t} = B(A+u) \left(\frac{v}{L_c} \right) \quad (9)$$

Rewriting (9) and integrating,

$$\int_0^u \frac{du}{A+u} = \frac{B}{L_c} \int_0^t v dt \quad (10)$$

Hence,

$$\ln \left(\frac{A+u}{A} \right) = \frac{BL}{L_c} \quad (11)$$

in which L represents the total length of chart traced out in time t .

Now $L/L_c = N_c$, the number of stress reversals in time t . Thus,

$$\ln \left(\frac{A+u}{A} \right) = BN_c \quad (12)$$

If U_{N_c} is the pore pressure after N_c stress reversals, then,

$$U_{N_c} = A [\exp(BN_c) - 1] \quad (13)$$

By fitting (13) to the recorded pore pressure trace, A and B can be determined. Equations (6) and (7) then enable values for p_c and M to be found.

In deriving this solution, it has been assumed that $u = 0$ when $t = 0$. A further two points on the measured trace must be used to solve (13) for A and B.

Having determined A and B (and hence p_c and M), equation (4) can be integrated to give the predicted mean u versus W response for different functional forms of the shear modulus $\mu = \mu(p)$. The following simple linear expression for μ will be used

$$\mu = (F - u)/a \quad (14)$$

where F is the measured pore pressure at failure and a is a constant.

$$\text{Letting } \Delta\sigma = \sigma_c - F \quad (15)$$

$$\text{gives } \mu = (p - \Delta\sigma)/a \quad (16)$$

Equation (14) is at best a first order approximation for the shear modulus of any sand. Its simplicity is an advantage however, and, as will be shown below, it appears sufficient to describe the experimental data fairly well. Substituting (16) in (4) gives,

$$\begin{aligned} \frac{du}{dW} &= \frac{(\sigma_c - u - p_c) (1 - \exp(-q_1^2/2M^2))}{\frac{aM^2}{4(F-u)} \left[\ln \left(\frac{1}{1 - (q_1/M)^2} \right) - \left(\frac{q_1}{M} \right)^2 \right]} \\ &= C (F-u) (\sigma_c - u - p_c) \end{aligned} \quad (17)$$

$$\text{where } C = \frac{4}{aM^2} \left\{ \frac{1 - \exp(-q_1^2/2M^2)}{\ln \left[\frac{1}{1 - (q_1/M)^2} \right] - \left(\frac{q_1}{M} \right)^2} \right\} \quad (18)$$

Now since the mean effective stress p equals $\sigma_c - u$, we have $dp = -du$, and (17) can be written,

$$\frac{dp}{dW} = C(p-\Delta\sigma) (p_c - p) \quad (19)$$

Integrating this equation gives,

$$W = \frac{-1}{C(p_c - \Delta\sigma)} \ln \left(\frac{p_c - p}{p - \Delta\sigma} \times \frac{\sigma_c - \Delta\sigma}{p_c - \sigma_c} \right) \quad (20)$$

Equation (20) gives the predicted u versus W response for the values of p_c and M determined from the pore pressure time history.

Typical Fitting of Results

Because of time limitations only 5 of the 32 records from the test program were completely reduced for comparison with the theory. Two tests run at each of 150 kPa and 100 kPa and one test at 50 kPa confining pressure were used in the comparison. A detailed development of the analysis of one of the tests follows.

Analysis of Test 6/12/80, Cell 1

In Chapter 3 the experimental results collected for this particular test were discussed. Figures 7, 8 and 9 presented the recorded responses of this sample.

The first step in the analysis of the test results was to find values for the constants A and B , as introduced in equations (6) and (7). To obtain these values, the pore pressure trace (Figure 7) was used. Fitting equation (13) to the measured pore pressure record requires the determination of the values of the pore pressure at two points. As the pore pressure within the sample is constantly changing in response to the applied load, it is necessary to decide on what is to be called the pore pressure value at any nominated cycle. As the theory discussed earlier applies only at zero load, the pore pressure value for any single load stroke (either one tension or one compression pulse) was determined at the point where the load pattern for that stroke returned to the zero load line. The pore pressure value for one complete cycle (one tension *and* one compression pulse) was determined by averaging the values measured for each stroke of that cycle.

For the test being analysed, the following results were obtained,

$$A = 160.644 \text{ kPa and } B = 0.026.$$

A summary of the fitting procedure and the fitted exponential curve is presented in Figure 13. The fitted pore pressure response, equation (13), was then plotted on the experimental u versus W trace to give the average response for this curve, (Figure 14). Note that the dashed line in this figure does not represent the theoretical u versus W response given by equation (20). Instead, the values of the average pore pressure at the end of each loading cycle have been plotted for the corresponding cycle number.

Having determined the constants, A and B , it is now possible to use equation (20) to calculate the predicted pore pressure - work response. From equations (6) and (7) we find that,

$$p_c = 260.6 \text{ kPa}, \quad M = 157.02 \text{ kPa}.$$

The constant C defined by equation (18) becomes,

$$C = -0.0031/a.$$

The experimentally measured mean pore pressure at failure is,

$$F = 70.5 \text{ kPa}.$$

Thus from equation (20) we have,

$$W = 1.3959 a \ln \left[0.4389 \left(\frac{160.644 + u}{70.5 + u} \right) \right] \quad (21)$$

This equation still contains one undetermined parameter, the value of a . The value of a reflects the shear compliance of the sample during testing. In general, theoretical u versus W plots were made for various values of a , as indicated in Figure 15. The close agreement between the theoretical and measured responses, particularly for the value of $a = 0.034$ is evident in this plot.

A Summary of Test Results

The procedure described above was carried out on the other four tests analysed. Figure 16 provides a summary of the theoretical and actual results for these four tests. Once again the theoretical responses appear to closely represent the measured responses.

The remaining 27 test records were analysed to determine the general trend of all results. Exponential curves, equation (13), were fitted, where possible, to the measured pore pressure traces, and a summary plot (Figure 17) drawn up for each of the confining pressures used. An average theoretical line from one of the analysed tests is also presented to indicate the degree of agreement between theory and the determined experimental results.

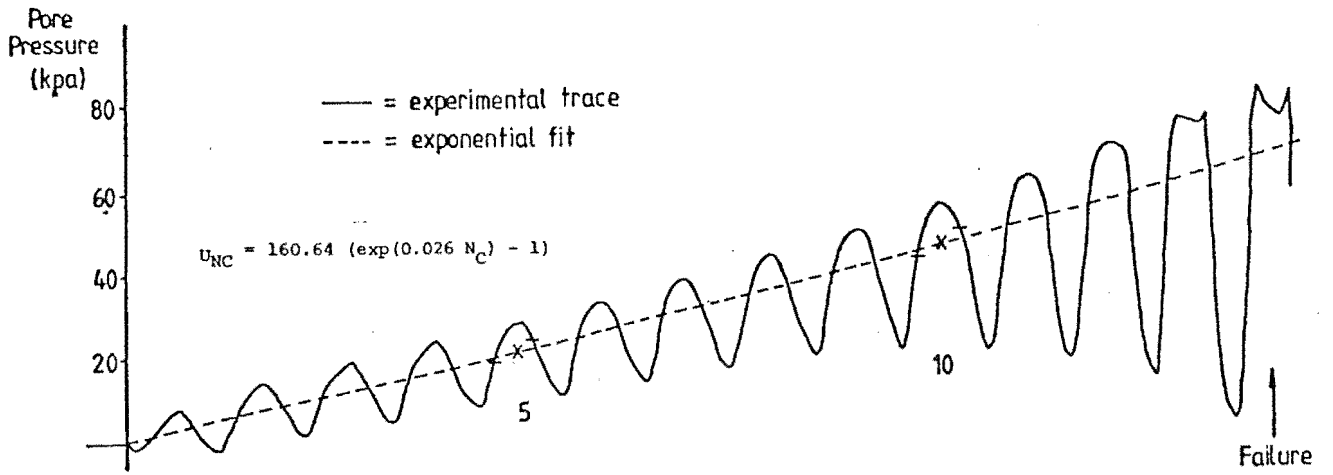


FIG. 13 A typical experimental pore pressure trace fitted with an exponential curve.

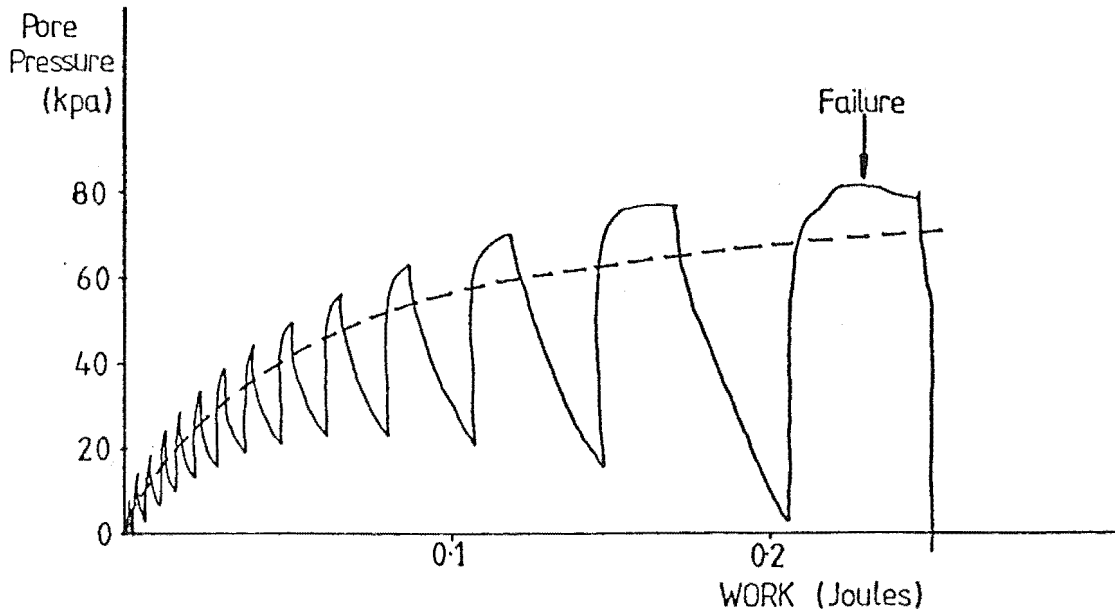


FIG. 14 The pore pressure versus work plot for a typical test, fitted with an average curve.

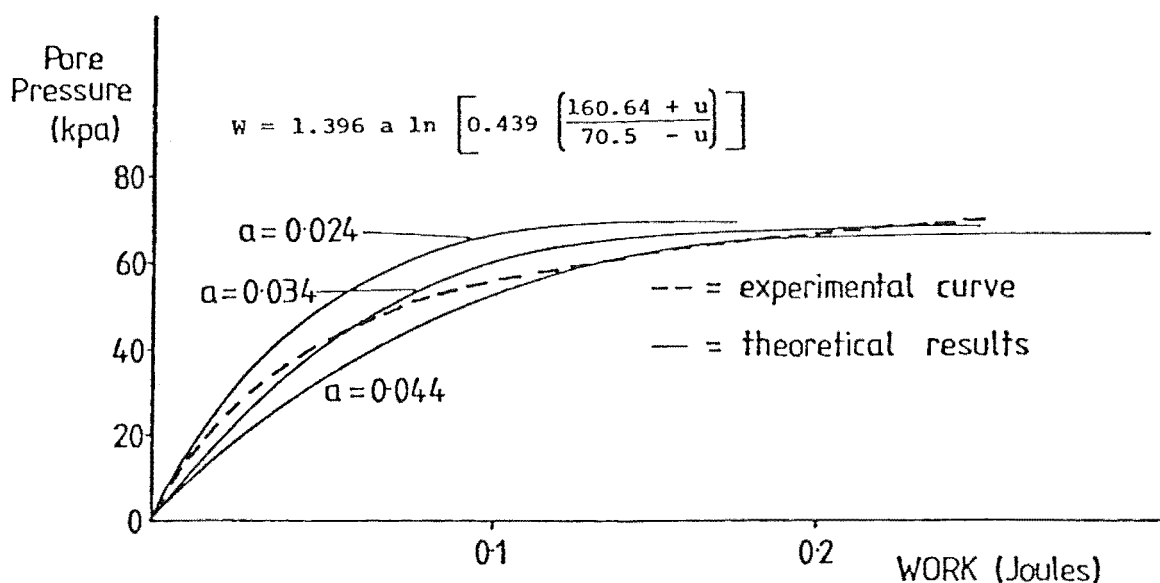


FIG. 15 A comparison of the theoretical pore pressure versus work relationship with the result recorded during a typical test.

Discussion

The comparison of experimental and predicted results indicates that some progress has been made in deriving a theory for the mechanism of liquefaction. Not all of the experimental records collected were used in carrying out this comparison, however. It was not possible to fit the exponential curve (equation (13)) through the pore pressure traces from 9 of the 32 tests. Although this appears to be a high proportion of the total number of tests conducted, there are several explanations for the particular behaviour recorded in these tests.

In two of the tests, problems were experienced with the pore pressure transducer. Electrical noise from water in the connections caused results which eliminates these two tests from consideration. However as the other pieces of recording equipment operated satisfactorily, the results could still be considered in the stage one analysis.

In three of the remaining seven tests, failure occurred within the first ten cycles. The gradual buildup of load, characteristic of the loading apparatus used, is particularly evident throughout the duration of these tests. As a result, the sample is subjected to a non-uniform extension and compression loading. The unequal loading correspondingly affects the pore pressure buildup, giving a response which was not exponential with time.

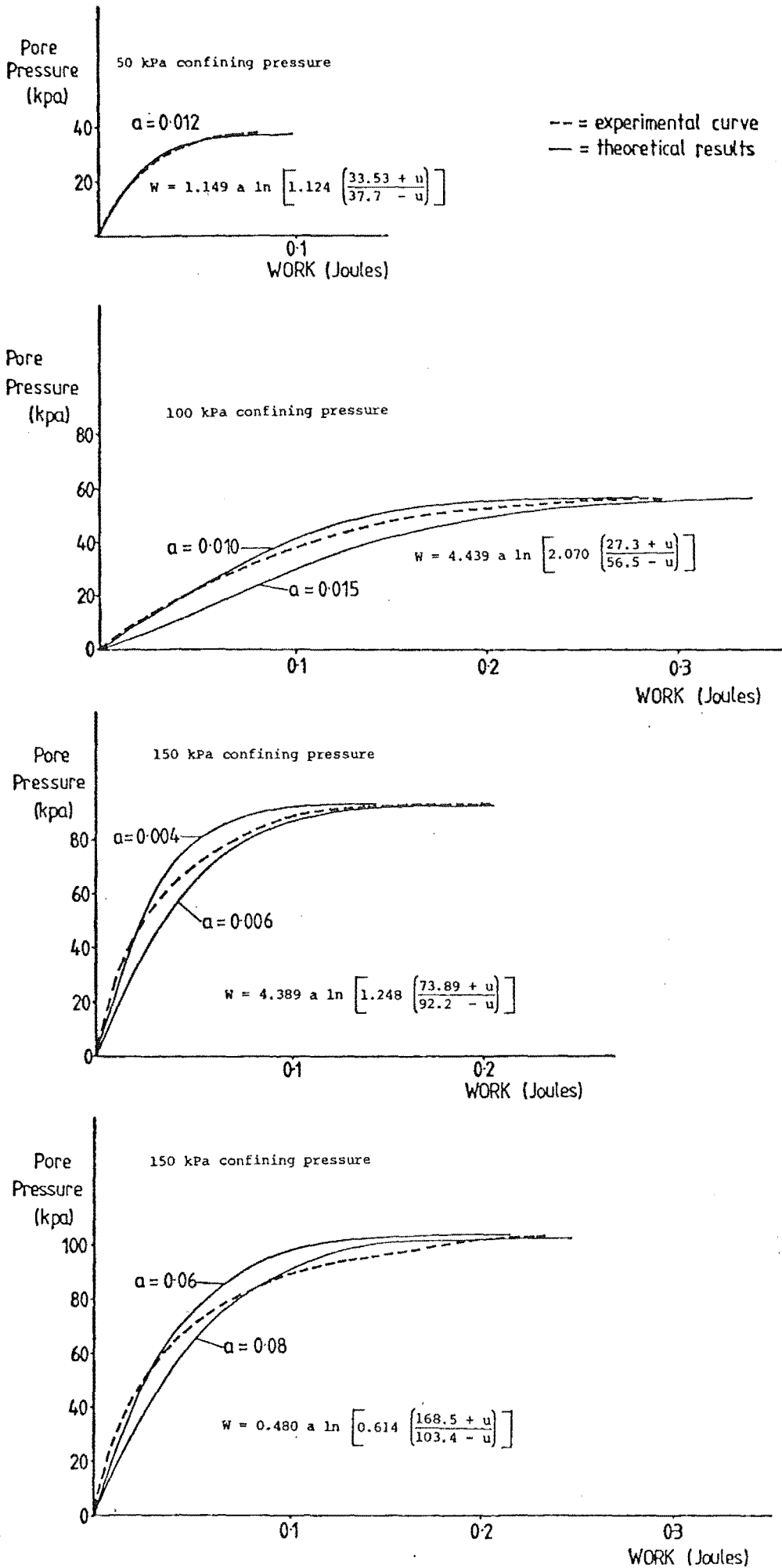


FIG. 16 Summary presentation of the theoretical and recorded pore pressure versus work traces for four analysed tests.

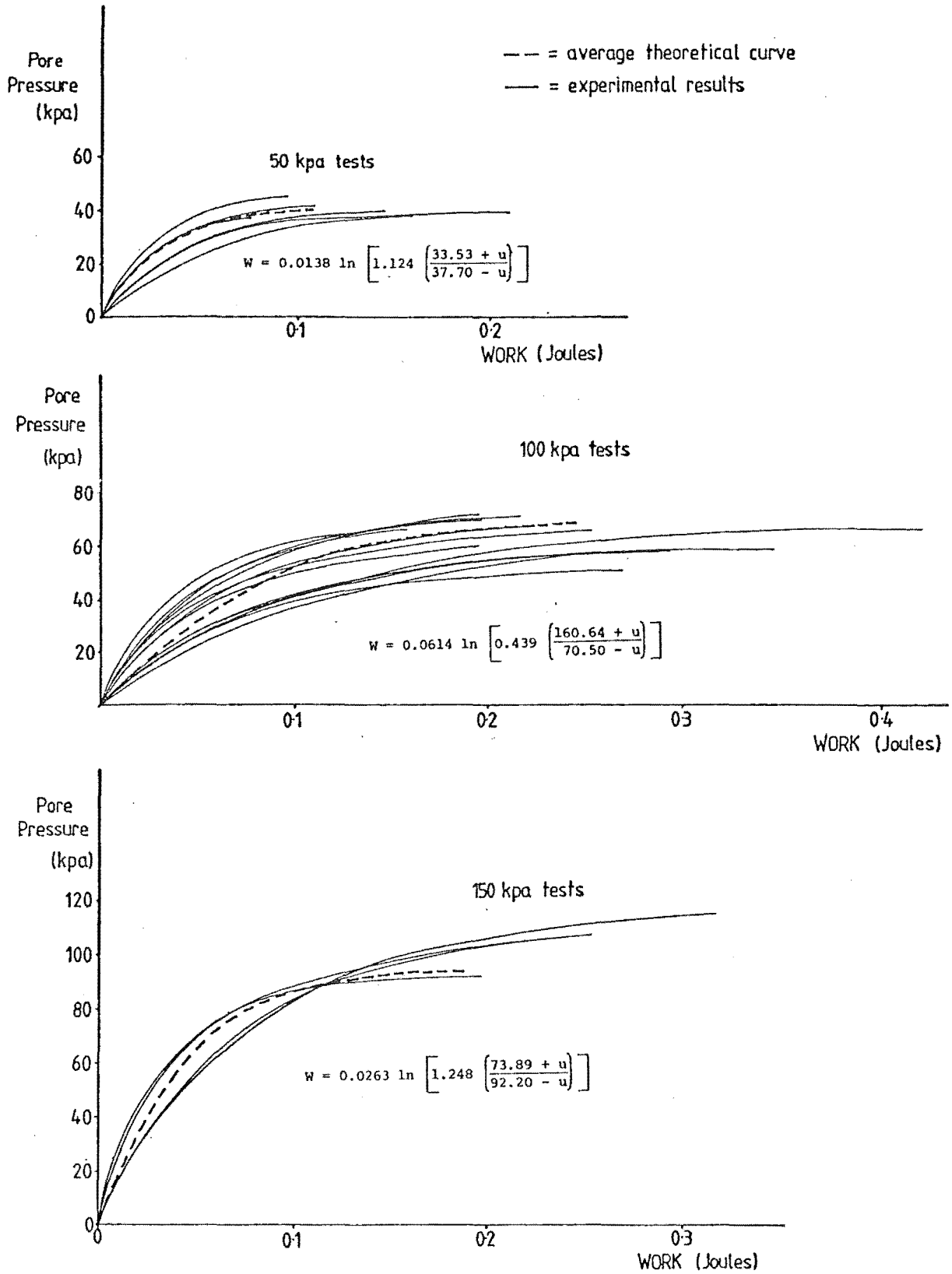


FIG. 17 Average pore pressure versus work traces for all recorded results. The theoretical results from the analysed tests are plotted where appropriate.

The remaining four tests which were not considered in the stage 2 analysis were all of greater than 50 cycles in duration, and run at cell pressures of 100 or 150 kPa. At these high confining pressures, some leakage of pore water was evident. This leakage was particularly apparent in cell number 3. It is considered to be more than coincidence that cell 3 was used in five of the nine invalid tests. Any such leakage within the pore water pressure measuring system effectively drains the sample, leaking some of the pressure that would otherwise be recorded as pore water pressure build-up. This leakage becomes more significant in longer duration tests. The leakage is also accelerated by the higher confining pressures acting on the sample in these tests. Consequently the pore water response to the applied loading is not exponential with time and does not fit the pattern predicted in equation (13).

Because of the low confining pressure, 50 kPa tests were more easily controlled. It is interesting to note that the exponential pore pressure fit (equation (17)) was possible in all tests at this confining pressure. The agreement between the two point fitted trace, and the actual recorded response is almost exact throughout the test duration for all six 50 kPa tests. Certainly, this series being the last attempted, and also the repair of the leakage problems discussed earlier contributed to the apparent consistency of response exhibited in these tests.

It was expected, before testing began, that the failure pore pressure would be approximately the same magnitude as the cell confining pressure. During testing it was discovered that in fact the samples failed at pore pressures 10-20% less than anticipated. The value of the failure pore pressure was consistent within $\pm 5\%$ for all tests run at the same nominal confining pressure. This consistency indicates that, within acceptable tolerances, sample properties and testing conditions were similar. However, as the failure pore pressures were somewhat lower than expected it is possible that the actual confining pressure in the cell was lower than the gauged value. Samples tested at 50 kPa confining pressure failed at higher relative pore pressures than those tested at 100 and 150 kPa. This further supports the idea of the difficulty in adequately managing higher cell confining pressures with the equipment used.

It was not of major concern that lower confining pressures than nominated may have been used in the testing program. The theory being investigated was related to the magnitude of the failure pore pressure and not the confining pressure. Consequently, provided the confining pressures were consistently above or below a nominated value, the test results recorded were adequate for the stage 2 analysis.

CONCLUSIONS

The particular procedure developed for the test program was effective in enabling the production and cyclic triaxial testing of sand samples of consistent properties and exhibiting consistent experimental behaviour. It was found to be important that samples be prepared with as little disturbance as possible, if the desired consistency of properties was to be achieved. The care and attention this required was characteristic of that necessary during all stages of the test procedure. In particular, it was critical that the alignment of the triaxial cell piston and the pneumatic loading ram be established to within very small tolerances. The test program further showed the feasibility of continuous digital integration of the ram force and sample deformation to yield the work done on the sample throughout the test.

The analysis of the experimental results to investigate the pore pressure to work relationship of a sample revealed a close agreement between the experimentally measured results and the response predicted by the simple theory outlined in Chapter 4.

Recommendations for Further Work

The work carried out in the investigation was exploratory in nature. The apparent agreement between the predicted and recorded results is indicative of the need for more detailed research along similar lines. This work would have the aim of establishing the relationship between pore pressure buildup, confining pressure and the dissipated energy, for all sands. Such a relationship could be used to replace the equivalent number of cycles ideas developed by Seed et al⁽¹⁰⁾ and enable the prediction of the pore pressure response to a given energy input for a sand at a known confining pressure.

REFERENCES

1. Seed, H. B., and Idriss, I. N., "Analysis of Soil Liquefaction - Niigata Earthquake". Journal Soil Mechanics and Foundation Division, ASCE, Vol.93, No.SM3: 83-108, 1967.
2. Hazan, A., "Hydraulic Fill Dams". ASCE Transactions, Vol.83: 1713-1745, 1920.
3. Seed, H. B., Lee, K. L., Idriss, I. N., Makdisi, F. I., "The Slides in the San Fernando Dams During the Earthquake of Feb. 7, 1971". Journal of the Geotechnical Engineering Division, ASCE, Vol. 101, No.GT7, July 1975.
4. Kishida, H., "Damage to Reinforced Concrete Buildings in Niigata City With Special Reference to Earth Engineering". Soils and Foundations, Vol.VII, No.1, 1976.
5. Koizumi, K., "Change in Density of Sand Subsoil Caused by the Niigata Earthquake". Soils and Foundations, Vol.VIII No.2: 38-44, 1966.
6. Ohsaki, Yorihiro., "Niigata Earthquakes, 1964, Building Damage and Soil Conditions". Soils and Foundations, Vol.VI, No.2: 14-37, 1966.
7. Seed, H. B., Peacock, William H., "Test Procedures for Measuring Soil Liquefaction Characteristics". Journal Soil Mechanics and Foundation Division, ASCE, Vol.97, No.SM8, Proc. Paper 8330, August 1971.
8. Finn, W.D.L., Lee, K. W., Martin, G. R., "Stress Strain Relationships for Sand in Simple Shear". ASCE National Convention, Denver Colorado, Meeting Reprint 2517, November 1975.
9. Finn, W. D. L., Lee, K. W., Martin, G. R., "An Effective Stress Model for Liquefaction". ASCE Annual Convention and Exposition, Philadelphia, Reprint 2752, September 1976.
10. Seed, H. B., Martin, P. P., Lysmer, John., "Pore Water Pressure Changes During Soil Liquefaction". Journal of the Geotechnical Engineering Division, ASCE, No.GT4:323-346, April 1976.
11. Oh-Oka, Hiroshi., "Drained and Undrained Stress-Strain Behaviour of Sands Subjected to Cyclic Shear Stress Under Nearly Plane Strain Conditions". Soils and Foundations, Vol.16, No.3, 1976.

12. Nemat-Nasser, S. and Shokooh, A., "A Unified Approach to Densification and Liquefaction of Cohesionless Sand in Cyclic Shearing". Canadian Geotechnical Journal, Vol.16, No.4: 659-679, 1979.
13. Davis, R. O. and Mullenger, G., "A Simple Rate Type Constitutive Representation for Granular Media". Proceedings Third International Conference on Numerical Methods in Geomechanics, Aachen, April 1979.
14. Roscoe, K. H. and Burland, J. B., "On the Generalised Stress Strain Behaviour of Wet Clay". In J. Heyman and F. A. Leckie (eds) Engineering Plasticity, Cambridge University Press, pp 535-609, 1968.
15. Chan, C. K., Mulilis, T. P., "Pneumatic Sinusoidal Loading System". Journal of the Geotechnical Engineering Division, ASCE, Vol. 102, No. GT3, Technical Notes, pp 277-282, 1976.
16. Silver, Marshall L. et al., "Cyclic Triaxial Strength of Standard Test Sand". Journal Geotechnical Engineering Division, ASCE, Vol.102, No. GT5, May 1976.
17. Ladd, R. S., "Preparing Test Specimens Using Undercompaction". Geotechnical Testing Journal, Vol.1, No.1: 16-23, March 1978.
18. Ferrito, J. M., Forrest, J. B., Wu, George., "A Compilation of Cyclic Triaxial Liquefaction Test Data". Geotechnical Testing Journal, Vol.2, No.2: 106-113, June 1979.
19. Mulilus, J. P., Townsend, F. C., Horz, R. C., "Triaxial Testing Techniques and Sand Liquefaction". Dynamic Geotechnical Testing, American Society for Testing and Materials, STP 654, pp 265-279, 1978.
20. Cho, Y., Rizzo, P. C., Humphries, W. K., "Saturated Sand and Cyclic Dynamic Tests". ASCE Annual Convention and Exposition Philadelphia, Preprint 2752, pp 285-312, September 1976.
21. Vickers, Brian., "Laboratory Work in Civil Engineering - Soil Mechanics". Granada Publication, pp 74-110.
22. Schofield, A. and Wroth C. P. "Critical State Soil Mechanics". McGraw Hill, New York, 1960.